

# Measurement of Charm Production Cross Sections in $e^+e^-$ Annihilation at Energies between 3.97 and 4.26 GeV

D. Cronin-Hennessy,<sup>1</sup> K. Y. Gao,<sup>1</sup> J. Hietala,<sup>1</sup> Y. Kubota,<sup>1</sup> T. Klein,<sup>1</sup> B. W. Lang,<sup>1</sup>  
R. Poling,<sup>1</sup> A. W. Scott,<sup>1</sup> P. Zweber,<sup>1</sup> S. Dobbs,<sup>2</sup> Z. Metreveli,<sup>2</sup> K. K. Seth,<sup>2</sup>  
A. Tomaradze,<sup>2</sup> J. Libby,<sup>3</sup> A. Powell,<sup>3</sup> G. Wilkinson,<sup>3</sup> K. M. Ecklund,<sup>4</sup> W. Love,<sup>5</sup>  
V. Savinov,<sup>5</sup> A. Lopez,<sup>6</sup> H. Mendez,<sup>6</sup> J. Ramirez,<sup>6</sup> J. Y. Ge,<sup>7</sup> D. H. Miller,<sup>7</sup>  
I. P. J. Shipsey,<sup>7</sup> B. Xin,<sup>7</sup> G. S. Adams,<sup>8</sup> M. Anderson,<sup>8</sup> J. P. Cummings,<sup>8</sup>  
I. Danko,<sup>8</sup> D. Hu,<sup>8</sup> B. Moziak,<sup>8</sup> J. Napolitano,<sup>8</sup> Q. He,<sup>9</sup> J. Insler,<sup>9</sup> H. Muramatsu,<sup>9</sup>  
C. S. Park,<sup>9</sup> E. H. Thorndike,<sup>9</sup> F. Yang,<sup>9</sup> M. Artuso,<sup>10</sup> S. Blusk,<sup>10</sup> S. Khalil,<sup>10</sup> J. Li,<sup>10</sup>  
R. Mountain,<sup>10</sup> S. Nisar,<sup>10</sup> K. Randrianarivony,<sup>10</sup> N. Sultana,<sup>10</sup> T. Skwarnicki,<sup>10</sup>  
S. Stone,<sup>10</sup> J. C. Wang,<sup>10</sup> L. M. Zhang,<sup>10</sup> G. Bonvicini,<sup>11</sup> D. Cinabro,<sup>11</sup> M. Dubrovin,<sup>11</sup>  
A. Lincoln,<sup>11</sup> J. Rademacker,<sup>12</sup> D. M. Asner,<sup>13</sup> K. W. Edwards,<sup>13</sup> P. Naik,<sup>13</sup> J. Reed,<sup>13</sup>  
R. A. Briere,<sup>14</sup> T. Ferguson,<sup>14</sup> G. Tatishvili,<sup>14</sup> H. Vogel,<sup>14</sup> M. E. Watkins,<sup>14</sup>  
J. L. Rosner,<sup>15</sup> J. P. Alexander,<sup>16</sup> D. G. Cassel,<sup>16</sup> J. E. Duboscq,<sup>16</sup> R. Ehrlich,<sup>16</sup>  
L. Fields,<sup>16</sup> L. Gibbons,<sup>16</sup> R. Gray,<sup>16</sup> S. W. Gray,<sup>16</sup> D. L. Hartill,<sup>16</sup> B. K. Heltsley,<sup>16</sup>  
D. Hertz,<sup>16</sup> C. D. Jones,<sup>16</sup> J. Kandaswamy,<sup>16</sup> D. L. Kreinick,<sup>16</sup> V. E. Kuznetsov,<sup>16</sup>  
H. Mahlke-Krüger,<sup>16</sup> D. Mohapatra,<sup>16</sup> P. U. E. Onyisi,<sup>16</sup> J. R. Patterson,<sup>16</sup>  
D. Peterson,<sup>16</sup> D. Riley,<sup>16</sup> A. Ryd,<sup>16</sup> A. J. Sadoff,<sup>16</sup> X. Shi,<sup>16</sup> S. Stroiney,<sup>16</sup>  
W. M. Sun,<sup>16</sup> T. Wilksen,<sup>16</sup> S. B. Athar,<sup>17</sup> R. Patel,<sup>17</sup> J. Yelton,<sup>17</sup> P. Rubin,<sup>18</sup>  
B. I. Eisenstein,<sup>19</sup> I. Karliner,<sup>19</sup> S. Mehrabyan,<sup>19</sup> N. Lowrey,<sup>19</sup> M. Selen,<sup>19</sup> E. J. White,<sup>19</sup>  
J. Wiss,<sup>19</sup> R. E. Mitchell,<sup>20</sup> M. R. Shepherd,<sup>20</sup> D. Besson,<sup>21</sup> and T. K. Pedlar<sup>22</sup>

(CLEO Collaboration)

<sup>1</sup>*University of Minnesota, Minneapolis, Minnesota 55455, USA*

<sup>2</sup>*Northwestern University, Evanston, Illinois 60208, USA*

<sup>3</sup>*University of Oxford, Oxford OX1 3RH, UK*

<sup>4</sup>*State University of New York at Buffalo, Buffalo, New York 14260, USA*

<sup>5</sup>*University of Pittsburgh, Pittsburgh, Pennsylvania 15260, USA*

<sup>6</sup>*University of Puerto Rico, Mayaguez, Puerto Rico 00681*

<sup>7</sup>*Purdue University, West Lafayette, Indiana 47907, USA*

<sup>8</sup>*Rensselaer Polytechnic Institute, Troy, New York 12180, USA*

<sup>9</sup>*University of Rochester, Rochester, New York 14627, USA*

<sup>10</sup>*Syracuse University, Syracuse, New York 13244, USA*

<sup>11</sup>*Wayne State University, Detroit, Michigan 48202, USA*

<sup>12</sup>*University of Bristol, Bristol BS8 1TL, UK*

<sup>13</sup>*Carleton University, Ottawa, Ontario, Canada K1S 5B6*

<sup>14</sup>*Carnegie Mellon University, Pittsburgh, Pennsylvania 15213, USA*

<sup>15</sup>*Enrico Fermi Institute, University of Chicago, Chicago, Illinois 60637, USA*

<sup>16</sup>*Cornell University, Ithaca, New York 14853, USA*

<sup>17</sup>*University of Florida, Gainesville, Florida 32611, USA*

<sup>18</sup>*George Mason University, Fairfax, Virginia 22030, USA*

<sup>19</sup>*University of Illinois, Urbana-Champaign, Illinois 61801, USA*

<sup>20</sup>*Indiana University, Bloomington, Indiana 47405, USA*

<sup>21</sup>*University of Kansas, Lawrence, Kansas 66045, USA*

<sup>22</sup>*Luther College, Decorah, Iowa 52101, USA*

(Dated: January 16, 2008)

## Abstract

Using the CLEO-c detector at the Cornell Electron Storage Ring, we have measured inclusive and exclusive cross sections for the production of  $D^+$ ,  $D^0$  and  $D_s^+$  mesons in  $e^+e^-$  annihilations at thirteen center-of-mass energies between 3.97 and 4.26 GeV. Exclusive cross sections are presented for final states consisting of two charm mesons ( $D\bar{D}$ ,  $D^*\bar{D}$ ,  $D^*\bar{D}^*$ ,  $D_s^+D_s^-$ ,  $D_s^{*+}D_s^-$ , and  $D_s^{*+}D_s^{*-}$ ) and for processes in which the charm-meson pair is accompanied by a pion. No enhancement in any final state is observed at the energy of the  $Y(4260)$ .

## I. INTRODUCTION

Hadron production in electron-positron annihilations just above  $c\bar{c}$  threshold has been a subject of mystery and little intensive study for more than three decades since the discovery of charm. Recent developments, like the observation of the  $Y(4260)$  reported by the BaBar collaboration [1] and subsequently confirmed by CLEO-c [2] and Belle [3], underscore our incomplete understanding and demonstrate the potential for discovery of new states, such as hybrids and glueballs. It is also clear that precise measurements of charm-meson properties will shed light on higher-energy investigations of  $b$ -flavored particles and new states that might decay into  $b$ . Charm decays also offer unique opportunities to test the validity and guide the development of theoretical tools, like lattice QCD, that are needed to interpret measurements of the CKM quark-mixing parameters [4]. Any comprehensive program of precise charm-decay measurements demands a detailed understanding of charm production.

Past studies of hadron production in the charm-threshold region have been largely measurements of the cross-section ratio  $R(s) = \sigma(e^+e^- \rightarrow \text{hadrons})/\sigma(e^+e^- \rightarrow \mu^+\mu^-)$  over this energy range that have been made by many experiments [5]. Recent measurements with the Beijing Spectrometer (BES) [6] near charm threshold are especially noteworthy. There is a rich structure in this energy region, reflecting the production of  $c\bar{c}$  resonances and the crossing of thresholds for specific charm-meson final states. Interesting features in the hadronic cross section between 3.9 and 4.2 GeV include a large enhancement at the threshold for  $D^*\bar{D}^*$  production (4.02 GeV) and a fairly large plateau that begins at  $D_s^{*+}D_s^-$  threshold (4.08 GeV). While there is considerable theoretical interest [7, 8, 9, 10], there has been little experimental information about the composition of these enhancements.

In this paper we describe measurements of charm-meson production in  $e^+e^-$  annihilations at thirteen center-of-mass energies between 3970 and 4260 MeV. These studies were carried out with the CLEO-c detector at the Cornell Electron Storage Ring (CESR) [11] in 2005-6. (Throughout this paper use of any particular mode implies use of the charge-conjugate mode as well.) The principal objective of the CLEO-c energy scan was to determine the optimal running point for studies of  $D_s^+$ -meson decays. The same data sample has been used to confirm the direct production of  $Y(4260)$  in  $e^+e^-$  annihilations and to demonstrate  $Y(4260)$  decays to final states in addition to  $\pi^+\pi^-J/\psi$  [2]. Specific results presented in this paper include cross-section measurements for exclusive final states with  $D^+$ ,  $D^0$  and  $D_s^+$  mesons and inclusive measurements of the total charm-production cross section and  $R(s)$ .

## II. DATA SAMPLE AND DETECTOR

The data sample for this analysis was collected with the CLEO-c detector. Both the fast-feedback analysis carried out as data were collected and the detailed analysis reported here are extensions of techniques developed for charm-meson studies at the  $\psi(3770)$  [12].

An initial energy scan, conducted during August-October, 2005, consisted of twelve energy points between 3970 and 4260 MeV, with a total integrated luminosity of  $60.0 \text{ pb}^{-1}$ . The scan was designed to provide cross-section measurements at each energy for all accessible final states consisting of a pair of charm mesons. At the highest energy point these include  $D\bar{D}$ ,  $D^*\bar{D}$ ,  $D^*\bar{D}^*$ ,  $D_s^+D_s^-$ ,  $D_s^{*+}D_s^-$ , and  $D_s^{*+}D_s^{*-}$ , where the first three include both charged and neutral mesons. A follow-up run beginning early in 2006 provided a larger sample of  $178.9 \text{ pb}^{-1}$  at 4170 MeV, not one of the original scan points, that proved essential in understanding the composition of charm production throughout this energy region.

The center-of-mass energies and integrated luminosities for the thirteen subsamples are listed in Table I. Integrated luminosity is determined by measuring the processes  $e^+e^- \rightarrow e^+e^-$ ,  $\mu^+\mu^-$ , and  $\gamma\gamma$  [13], which are used because their cross sections are precisely determined by QED. Each of the three final states relies on different components of the detector, with different systematic effects. The three individual results are combined using a weighted average to obtain the luminosity used for this analysis.

CLEO-c is a general-purpose magnetic spectrometer with most components inherited from the CLEO III detector [14], which was constructed primarily to study  $B$  decays at the  $\Upsilon(4S)$ . Its cylindrical charged-particle tracking system covers 93% of the full  $4\pi$  solid angle and consists of a six-layer all-stereo inner drift chamber and a 47-layer main drift chamber. These chambers are coaxial with a superconducting solenoid that provides a uniform 1.0-Tesla magnetic field throughout the volume occupied by all active detector components used for this analysis. Charged particles are required to satisfy criteria ensuring successful fits and vertices consistent with the  $e^+e^-$  collision point. The resulting momentum resolution is  $\sim 0.6\%$  at 1 GeV/ $c$  for tracks that traverse all layers of the drift chamber. Oppositely-charged and vertex-constrained pairs of tracks are identified as  $K_S^0 \rightarrow \pi^+\pi^-$  candidates if their invariant mass is within 4.5 standard deviations ( $\sigma$ ) of the known mass ( $\sim 12$  MeV/ $c^2$ ).

The main drift chamber also provides  $dE/dx$  measurements for charged-hadron identification, complemented by a Ring-Imaging Cherenkov (RICH) detector covering 80% of  $4\pi$ . The rate of pions faking kaons is  $(1.10 \pm 0.37)\%$ , with a pion identification efficiency for tracks in the RICH of  $(94.5 \pm 0.4)\%$ . The rate of kaons faking pions is  $(2.47 \pm 0.38)\%$ , with a kaon identification efficiency for tracks in the RICH of  $(88.4 \pm 0.6)\%$ .

An electromagnetic calorimeter consisting of 7784 CsI(Tl) crystals provides electron identification and neutral detection over 93% of  $4\pi$ , with photon-energy resolution of 2.2% at 1 GeV and 5% at 100 MeV. We select  $\pi^0$  and  $\eta$  candidates from pairs of photons with invariant masses within  $3\sigma$  of the known values [5] ( $\sigma \sim 6$  MeV/ $c^2$  for  $\pi^0$  and  $\sigma \sim 12$  MeV/ $c^2$  for  $\eta$ ).

TABLE I: Center-of-mass energies and integrated luminosity totals for all data samples used in this paper.

$E_{\text{cm}}$ (MeV)	$\int \mathcal{L} dt$ (pb $^{-1}$ )
3970	3.85
3990	3.36
4010	5.63
4015	1.47
4030	3.01
4060	3.29
4120	2.76
4140	4.87
4160	10.16
4170	178.89
4180	5.67
4200	2.81
4260	13.11

TABLE II: The decay modes and branching fractions used in determining the  $D_s$  cross sections.

Modes	$\mathcal{B}$ (%)
$K^+ K^- \pi^+$ , $ M_{KK} - M_\phi  < (10 \text{ MeV}/c^2)$ [15]	$1.99 \pm 0.11$
$\bar{K}^{*0} K^+, \bar{K}^{*0} \rightarrow K^- \pi^+$ [5]	$2.2 \pm 0.6$
$\eta \pi^+, \eta \rightarrow \gamma\gamma$ [5, 15]	$0.62 \pm 0.08$
$\eta \rho^+, \eta \rightarrow \gamma\gamma, \rho^+ \rightarrow \pi^+ \pi^0$ [5]	$4.3 \pm 1.2$
$\eta' \pi^+, \eta' \rightarrow \pi^+ \pi^- \eta, \eta \rightarrow \gamma\gamma$ [5, 15]	$0.66 \pm 0.07$
$\eta' \rho^+, \eta' \rightarrow \pi^+ \pi^- \eta, \eta \rightarrow \gamma\gamma, \rho^+ \rightarrow \pi^+ \pi^0$ [5]	$1.8 \pm 0.5$
$\phi \rho^+, \phi \rightarrow K^+ K^-, \rho^+ \rightarrow \pi^+ \pi^0$ [5]	$3.4 \pm 1.2$
$K_S K^+, K_S \rightarrow \pi^+ \pi^-$ [5, 15]	$1.03 \pm 0.06$

### III. EVENT-SELECTION PROCEDURES

The procedures and specific criteria for the selection of  $D^+$ ,  $D^0$  and  $D_s^+$  mesons closely follow previous CLEO-c analyses and are described in Refs. [12] and [15]. Candidates are identified based on their invariant masses and total energies, with selection criteria optimized on a mode-by-mode basis. We use only the cleanest final states for  $D^0$  ( $K^- \pi^+$ ) and  $D^+$  ( $K^- \pi^+ \pi^+$ ) selection, since these provide sufficient statistics for precise cross-section determinations. For  $D_s^+$  we optimize for efficiency by selecting the eight decay modes listed in Table II. Accepted intermediate-particle decay modes (mass cuts) are  $\phi \rightarrow K^+ K^-$  ( $\pm 10$  MeV),  $\bar{K}^{*0} \rightarrow K^- \pi^+$  ( $\pm 75$  MeV),  $\eta' \rightarrow \eta \pi^+ \pi^-$  ( $\pm 10$  MeV), and  $\rho^+ \rightarrow \pi^+ \pi^0$  ( $\pm 150$  MeV).

To determine the production yields and cross sections for the final states accessible at a particular center-of-mass energy, we classify events based on the energy and momentum of  $D_{(s)}$  candidate in the form of energy difference ( $\Delta E \equiv E_{D_{(s)}} - E_{\text{beam}}$ ) and beam-constrained mass ( $M_{\text{bc}} \equiv \sqrt{E_{\text{beam}}^2 - |\vec{P}_{D_{(s)}}|^2}$ ). Fig. 1 shows the expected behavior in a two-dimensional plot of  $\Delta E$  vs.  $M_{\text{bc}}$  for a Monte Carlo simulation of CLEO-c data at 4160 MeV with about

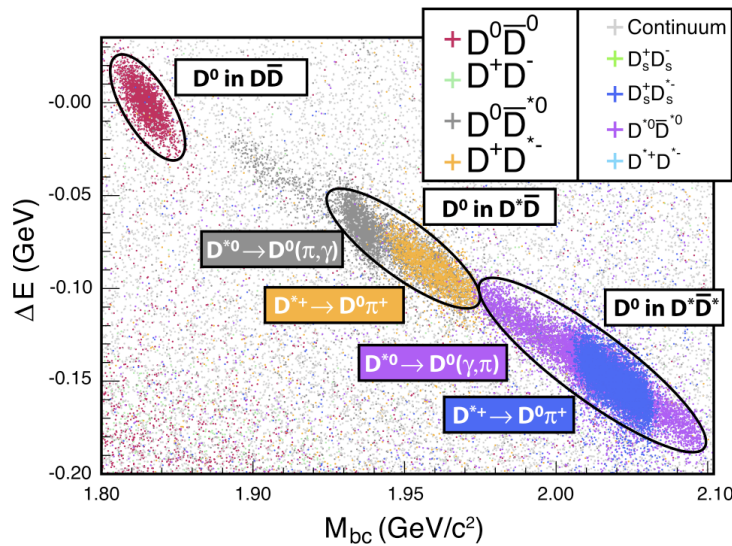


FIG. 1:  $\Delta E$  vs.  $M_{\text{bc}}$  in a Monte Carlo simulation of CLEO-c data at a center-of-mass energy of 4160 MeV, showing clear separation among the expected two-charm-meson final states.

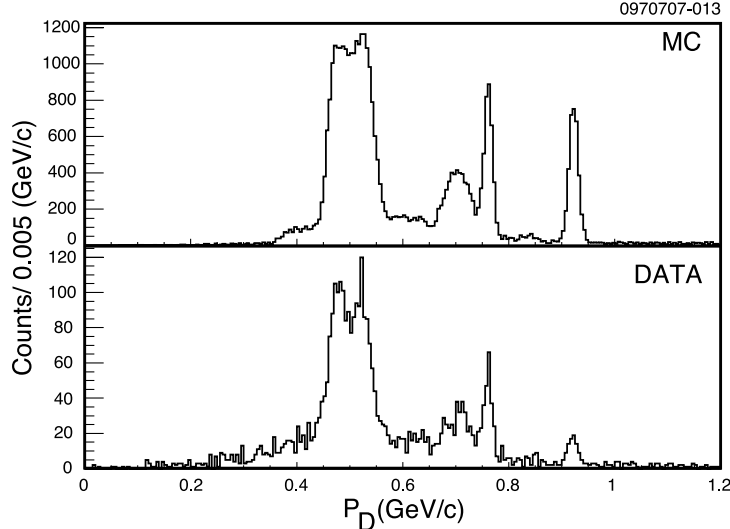


FIG. 2: Momentum spectra in Monte Carlo (top) and data (bottom) at 4160 MeV for  $D^0 \rightarrow K^- \pi^+$  candidates with an invariant mass within 15 MeV of the nominal value. As described in the text, the concentrations of entries correspond to expected final states with two charm mesons.

ten times the statistics of our data sample at that energy. There is clear separation of events among the expected final states consisting of two charm mesons. This separation was exploited during the scan run for a fast-feedback “cut-and-count” determination of event yields. It is also evident in plots of the momenta of charm-meson candidates selected by cutting on candidate invariant mass that the composition of final states can be analyzed by fitting the momentum spectra of  $D^0$ ,  $D^+$  and  $D_s^+$  candidates. Fig. 2 illustrates this with the momentum spectra for  $D^0 \rightarrow K^- \pi^+$  candidates within 15 MeV of the nominal mass both in the Monte Carlo sample of Fig. 1 and in  $10.16 \text{ pb}^{-1}$  of CLEO-c data at 4160 MeV. While no background corrections have been applied to these distributions, the structure of distinct Doppler-smeared peaks corresponding to different final states is evident. The Monte Carlo and data show good qualitative agreement, with concentrations of events corresponding to prominent final states near  $0.95 \text{ GeV}/c$  ( $D\bar{D}$ ),  $0.73 \text{ GeV}/c$  ( $D^* \bar{D}$ ) and  $0.5 \text{ GeV}/c$  ( $D^* \bar{D}^*$ ).

The cross sections for all contributing final states can be determined by correcting the raw measured momentum spectra like Fig. 2 for combinatoric and other backgrounds and then fitting to Monte Carlo predictions of the spectra. To achieve good fits, all significant production mechanisms must be included and the spectra predicted by Monte Carlo must reflect correct  $D^*$ -decay angular distributions and the effects of initial state radiation (ISR).

#### IV. EVIDENCE FOR MULTI-BODY PRODUCTION

While the qualitative features of the measured charm-meson momentum spectra accorded with expectations (Fig. 2), initial attempts to fit the spectra did not produce acceptable results. It was quickly concluded that the two-body processes listed above are insufficient to account for all observed charm-meson production. Final states like  $D\bar{D}^{(*)}\pi(\pi \dots)$ , in which the charm-meson pair is accompanied by one or more additional pions, emerged as the likely explanation. While not unexpected, these “multi-body” events have not previously been observed in the charm-threshold region, and there are no predictions of the cross sections

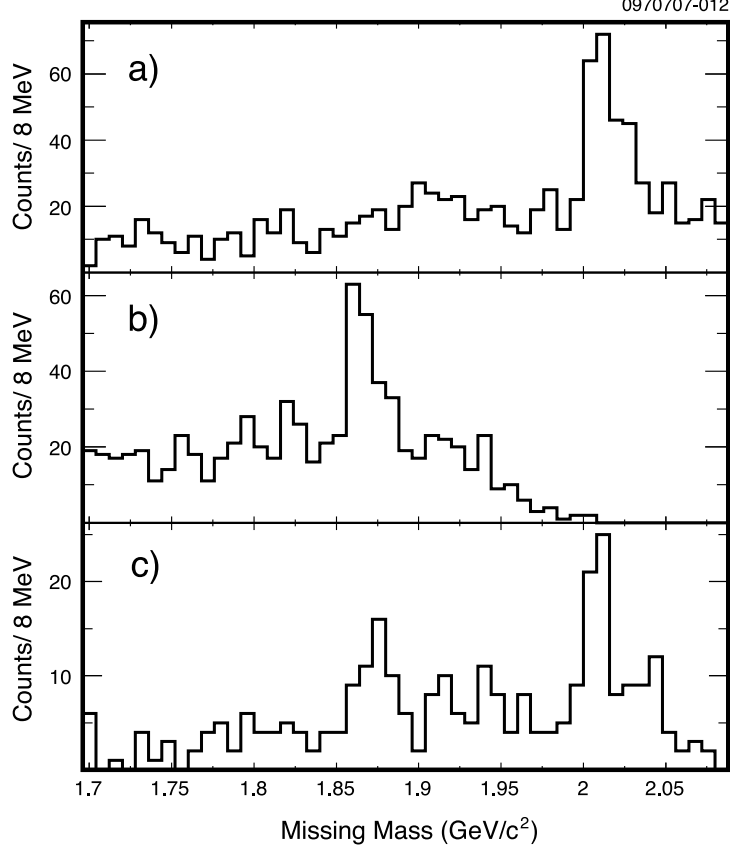


FIG. 3: The mass spectrum of  $X$  in (a)  $e^+e^- \rightarrow D^0\pi^\pm X$  at 4170 MeV, (b)  $e^+e^- \rightarrow D^{*\pm}\pi^\mp X$  at 4170 MeV, and (c)  $e^+e^- \rightarrow D^{*0}\pi^\pm X$  at 4260 MeV. Peaks at the  $D^*$  mass in (a) and the  $D$  mass in (b) are evidence for the decay  $D^*\bar{D}\pi$ . The  $D$  peak in (c) confirms  $D^*\bar{D}\pi$  and the  $D^*$  peak demonstrates that  $D^*\bar{D}^*\pi$  is produced at 4260 MeV.

for  $D^0$  and  $D^+$  production through multi-body final states.

To assess which multi-body final states ( $D\bar{D}\pi$ ,  $D^*\bar{D}\pi$ , etc.) are measurably populated in our data, we examine observables other than the charm-meson momenta, because ISR causes smearing of the peaks in the momentum spectra that can obscure the two-body kinematics. We applied  $D^{(*)}$  momentum selection criteria to exclude two-body contributions and examined the distributions of missing mass against a  $D^{(*)}$  and an accompanying charged or neutral pion, using charge correlations to suppress incorrect combinations. Fig. 3 shows clear evidence for  $D^*\bar{D}\pi$  events at 4170 MeV, as well as indications of  $D^*\bar{D}^*\pi$  in the sample of  $13 \text{ pb}^{-1}$  collected at 4260 MeV (Fig. 3c). These events cannot be attributed to two-body production with ISR, because radiative photons would destroy any peaking in the missing-mass spectrum. The absence of a peak at the  $D$  mass in Fig. 3a indicates that there is no evidence for  $D\bar{D}\pi$  production. Analysis of events with  $D_s$  reveals no evidence for multi-body production, consistent with expectations, since the  $D_s^+ D_s^- \pi^0$  final state violates isospin conservation.

## V. MOMENTUM-SPECTRUM FITS AND CROSS-SECTION RESULTS

Momentum spectra for  $D^0$ ,  $D^+$  and  $D_s^+$  candidates were found by requiring the invariant mass of  $D_{(s)}$  decay products to be within  $\pm 15$  MeV of the nominal value. Backgrounds are estimated with a sideband technique. Sideband regions are taken on both sides of the expected signal, and are significantly larger than the signal region to minimize statistical uncertainty in the background subtraction. Sideband widths are set mode by mode based on expectations for specific background processes.

Having identified the components of multi-body charm production, we determine yields for these channels and the two-body modes by fitting the sideband-subtracted  $D^0$ ,  $D^+$  and  $D_s^+$  momentum spectra. Signal momentum distributions for specific channels are based on full **GEANT** [16] simulations using **EvtGen** [17] for the production and decay of charm mesons. The **EvtGen** simulation incorporates all angular correlations by using individual amplitudes for each node in the decay chain. ISR is included in the simulation, which requires input of energy-dependent cross sections for each final state. We used simple parameterizations of these cross sections constructed by linearly interpolating between the preliminary measurements from our analysis. (In doing this we made the assumption that the energy dependence of the Born-level cross sections is adequately represented by the uncorrected cross sections.) For the multi-body  $D^*\bar{D}\pi$  and  $D^*\bar{D}^*\pi$  final states we used a spin-averaged phase-space model within **EvtGen**.

The momentum-dependent yields and fits to the relatively large sample of data at 4170 MeV are shown in Fig. 4 for (a)  $D^0 \rightarrow K^-\pi^+$ , (b)  $D^+ \rightarrow K^-\pi^+\pi^+$ , and (c)  $D_s^+ \rightarrow \phi\pi^+$  candidates. The lack of  $D_s^+$  entries below  $\sim 200$  MeV confirms the absence of multi-body  $D_s$  production. Because of the relative simplicity of  $D_s$  production, demonstrated by the  $D_s^+ \rightarrow \phi\pi^+$  fits, and the limited statistics of the sample, we determine the final cross sections for  $D_s^+D_s^-$ ,  $D_s^{*+}D_s^-$ , and  $D_s^{*+}D_s^{*-}$  by using a sideband-subtraction technique to count signal events in a region of the  $M_{bc} - \Delta E$  plane. The cross sections are then determined from a weighted sum of the yields for the eight  $D_s$  decay modes given in Table II, with weights minimizing the combined statistical and systematic uncertainties calculated from previously measured branching fractions and efficiencies determined by Monte Carlo. The cut-and-count analysis gives results that are consistent with momentum fits. There is good agreement among the separately-calculated cross sections for the different  $D_s$  decay modes.

Each of the thirteen data subsamples has been analyzed with the techniques developed and refined on data at 4170 MeV. A complete set of fit results is provided in Ref. [18]. Fig. 5 shows the  $D^0$ ,  $D^+$  and  $D_s$  fits for data sample at 4260 MeV, which are of particular interest because the charm-production cross sections might provide insight to the nature of the  $Y(4260)$  state. The fits at 4260 MeV behave similarly to those at lower energy, although a larger proportion of multi-body decays is apparent.

Cross sections for the two-body and multi-body final states are shown in Fig. 6. The uncertainties on the data points are statistical and systematic combined in quadrature. Ref. [18] provides detailed descriptions of the systematic uncertainties of the cross-section determinations. Briefly, there are three sources of systematic uncertainty: determination of the efficiency of charm-meson selection, extraction of yields, and overall normalization. The total systematic uncertainty (Table III) is not dominated by any one of these.

Track selection and particle identification closely follow previous CLEO-c analyses [12, 15]. The efficiency for reconstructing charged tracks has been estimated by a missing-mass technique applied to events collected at the  $\psi(2S)$  and  $\psi(3770)$  resonances. There is good



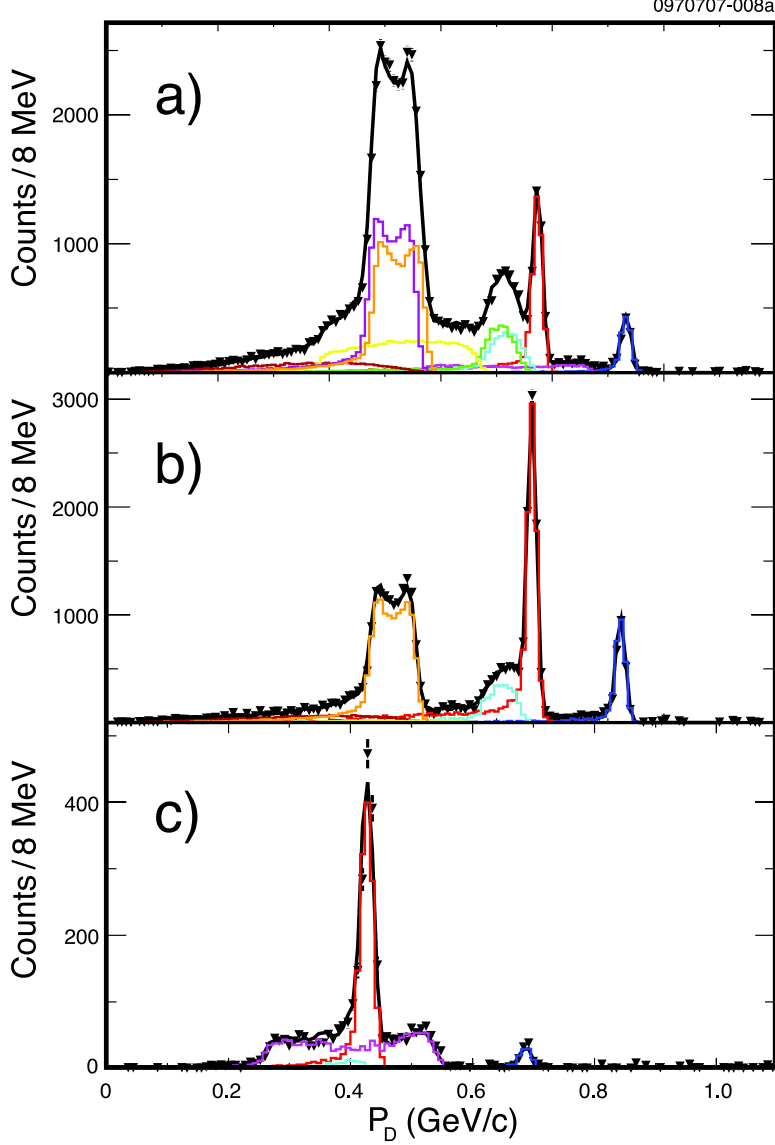


FIG. 4: Sideband-subtracted momentum spectra for (a)  $D^0 \rightarrow K^- \pi^+$ , (b)  $D^+ \rightarrow K^- \pi^+ \pi^+$ , and (c)  $D_s^+ \rightarrow \phi \pi^+$  at 4170 MeV. Data are shown as points with errors and the total fit result is shown as the solid black line. The colored histograms represent specific  $D_{(s)}$ -production mechanisms, with shapes obtained from Monte Carlo simulations and normalizations determined by the fits. For example, the primary  $D^0$  in  $D^{*0} \bar{D}^0$ , which peaks at 0.7 GeV/c, is shown in bright red. The secondary  $D^0$  mesons from the primary  $D^{*0}$  decaying via the emission of a  $\pi^0$  form the broad peak at 0.6 GeV/c shown in light blue. The second broad peak, at 0.6 GeV/c, consists of  $D^0$  mesons from the charged pion decay of the  $D^{*+}$  in  $D^{*+} D^-$ . All sources of multi-body events are combined and result in the broad spectrum between 0 and 0.5 GeV/c shown in dark red.

agreement between data and Monte Carlo, with an estimated relative uncertainty of  $\pm 0.7\%$  per track. Pion and kaon identification has been studied with  $D^0$  and  $D^+$  decays in  $\psi(3770)$  data, with estimated systematic uncertainties in the respective efficiencies of  $\pm 0.3\%$  and  $\pm 1.3\%$ . The uncertainties on reconstruction efficiencies for the neutral particles  $\pi^0$  and  $\eta$  for  $D_s$  decays have been estimated at  $\pm 2\%$  and  $\pm 4\%$ , respectively.

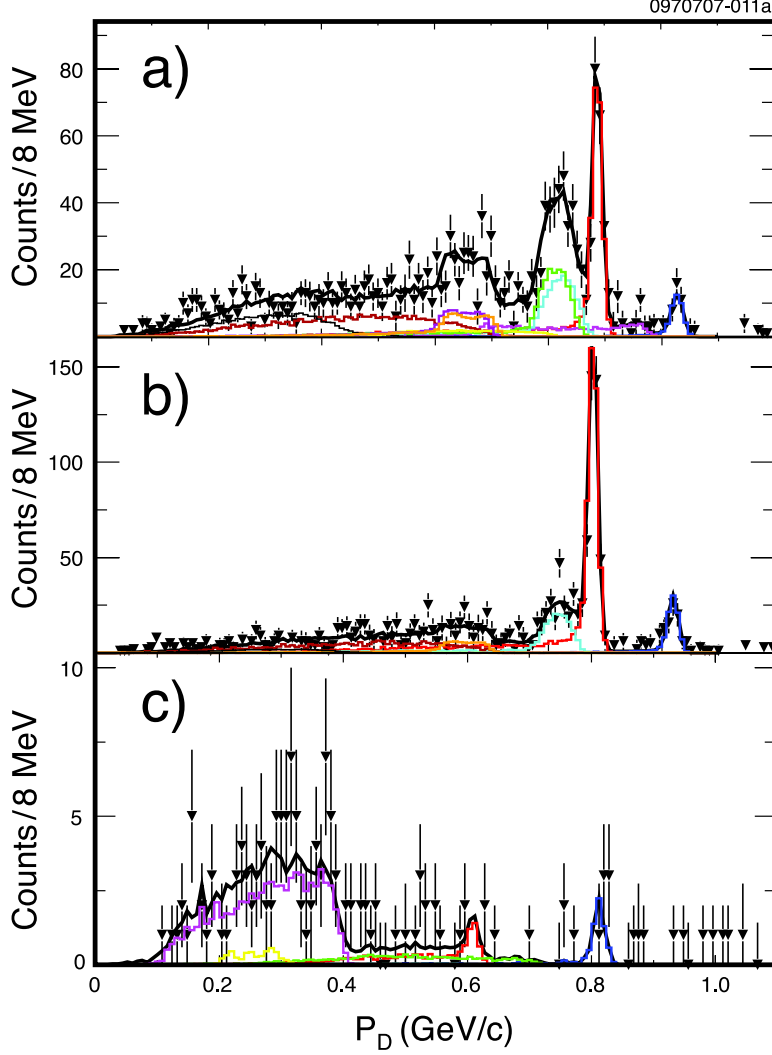


FIG. 5: Sideband-subtracted momentum spectra for (a)  $D^0 \rightarrow K^-\pi^+$ , (b)  $D^+ \rightarrow K^-\pi^+\pi^+$ , and (c)  $D_s^+ \rightarrow \phi\pi^+$  at 4260 MeV. Data are shown as points with errors and the total fit result is shown as the solid black line. The colored histograms represent fit components, mostly single  $D_{(s)}$ -production modes. For example, the primary  $D^0$  in  $D^{*0}\bar{D}^0$ , which peaks at 0.8 GeV/c, is shown in bright red. The secondary  $D^0$  mesons from the primary  $D^{*0}$  decaying via the emission of a  $\pi^0$  form the broad peak at 0.7 GeV/c shown in light blue. The second broad peak, at 0.7 GeV/c, consists of  $D^0$  mesons from the charged pion decay of the  $D^{*+}$  in  $D^{*+}D^-$ . The multi-body events are combined and result in the broad spectra between 0 and 0.6 GeV/c for  $D^*\bar{D}\pi$  (dark red) and between 0 and 0.4 GeV/c for  $D^*\bar{D}^*\pi$  (black).

The extraction of event yields by fitting the charm-meson momentum spectra (non- $D_s$  modes) incurs systematic uncertainty primarily through the signal functions generated by Monte Carlo, which depend on details of ISR and, in the case of  $D^*\bar{D}^*$ , the helicity amplitudes [18] and resulting  $D$ -meson angular distributions. As for the exclusive measurements, these details were studied with the large data sample at 4170 MeV, for which statistical uncertainties are small, and the resulting estimated relative systematic uncertainties are applied to all energy points. For the ISR calculation, the exclusive cross sections input to

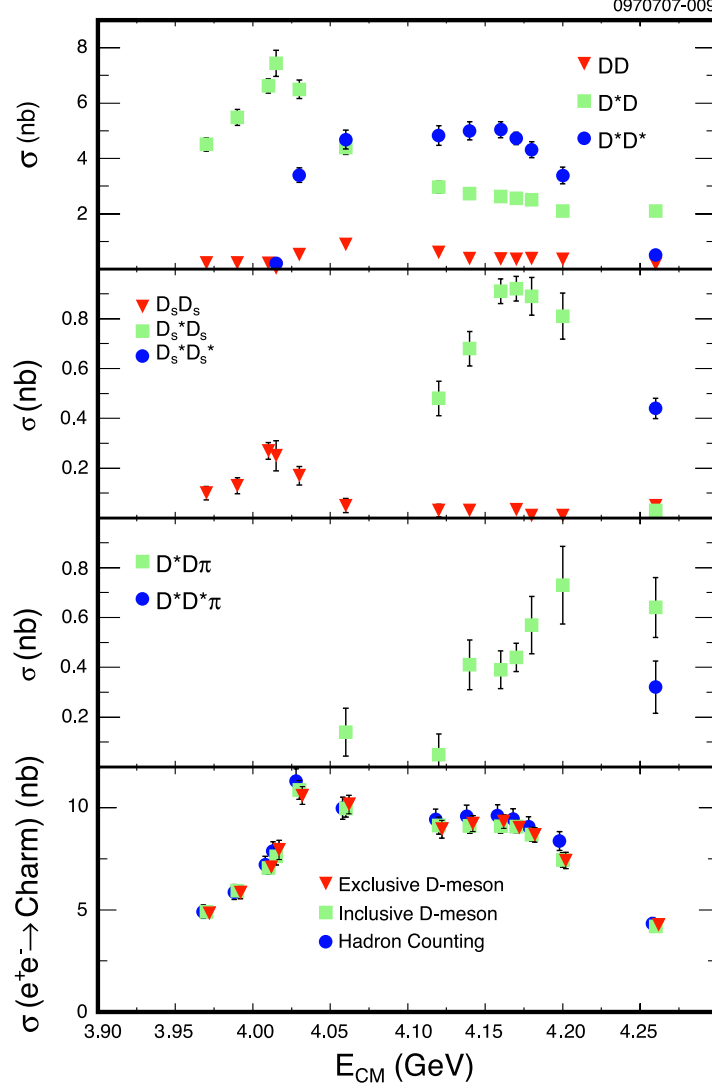


FIG. 6: Exclusive cross sections for two-body and multi-body charm-meson final states, and total observed charm cross section with combined statistical and systematic uncertainties.

**EvtGen** were varied from their nominal shapes. While a qualitative constraint of consistency with our measured cross sections was imposed, some extreme variations are included in the final systematic uncertainty. Both the direct effect on the fitted yield of varying a specific mode and the indirect effect of varying other modes were computed, although the former dominates in quadrature.

The yields for  $D_s$  final states are determined by direct counts after cutting on  $M_{bc}$  and  $\Delta E$ . Systematic uncertainty arises in these measurements if the Monte Carlo simulation does not provide an accurate determination of the associated efficiency. This is probed by adjusting the selection criteria and recomputing the cross sections, again using the high-statistics sample at 4170 MeV. The systematic uncertainties assigned based on these studies are  $\pm 3\%$ ,  $\pm 2.5\%$  and  $\pm 5\%$  for  $D_s^+ D_s^-$ ,  $D_s^{*+} D_s^-$ , and  $D_s^{*+} D_s^{*-}$ , respectively.

In converting the measured yields to cross sections we must correct for the branching fractions of the charm-meson decay modes. For each of the non-strange charm mesons,

TABLE III: Total systematic errors on the exclusive cross sections.

Mode	Relative Error ( $10^{-2}$ )
Determined by Momentum Fits	
$D\bar{D}$	4.5
$D\bar{D}^*$	3.4
$D^*\bar{D}^*$	4.7
$D^*\bar{D}\pi$	12.0
$D^*\bar{D}^*\pi$	25.0
Determined by Counting	
$D_s^+D_s^-$	5.6
$D_s^+D_s^{*-}$	5.3
$D_s^{*+}D_s^{*-}$	6.8

only one mode is used and CLEO-c measurements [12] provide the branching fractions and uncertainties:  $\pm 3.1\%$  for  $D^0 \rightarrow K^-\pi^+$  and  $\pm 3.9\%$  for  $D^+ \rightarrow K^-\pi^+\pi^+$ . For  $D_s$  modes we use CLEO-c measurements of the branching fractions for the eight decay modes included in the weighted sum [15]. The world-average value is used for the  $D^{*+} \rightarrow D^0\pi^+$  branching fraction, with a systematic uncertainty of  $\pm 0.7\%$  [5]. Finally, the cross-section normalization also depends on the absolute determination of the integrated luminosity for each data sample, with a systematic uncertainty of  $\pm 1.0\%$  [13].

A mode-by-mode summary of the systematic uncertainties in the exclusive cross-section measurements is provided in Table III. The systematic errors are 100% correlated across energy.

The cross-section measurements are presented in Tables IV, V, VI (modes with only two charm mesons), and VII (multi-body modes).

As a cross-check, for the two largest data samples (4170 MeV and 4260 MeV), the multi-body cross sections are also determined by fitting the distributions of missing mass against detected  $D^0\pi$ ,  $D^+\pi$  and  $D^*\pi$  combinations. While these measurements are less precise, they show good agreement with the results of the momentum-spectrum fits.

## VI. INCLUSIVE CROSS-SECTION MEASUREMENTS

If all final states have been included, the sum of the exclusive cross sections should equal the total charm cross section. We test this supposition with two inclusive measurements that can also be compared with past results.

The first cross-check is a measurement of the total charm-meson cross section:

$$\sigma(e^+e^- \rightarrow D\bar{D}X) = \frac{\sigma_{D^0} + \sigma_{D^+} + \sigma_{D_s^+}}{2}, \quad (1)$$

where the contributing cross sections are defined by  $\sigma_D = N_D/\epsilon B\mathcal{L}$ , where  $\epsilon$  and  $B$  are the efficiency and branching fraction for the decay mode used ( $D^0 \rightarrow K^-\pi^+$ ,  $D^+ \rightarrow K^-\pi^+\pi^+$ , and  $D_s^+ \rightarrow K^-K^+\pi^+$ ),  $\mathcal{L}$  is the integrated luminosity, and  $N_D$  is the yield obtained by fitting the mass spectrum. In the case of  $D^0$  and  $D^+$ , the invariant-mass distribution is fitted to a Gaussian signal and polynomial background. For  $D_s$ , the event-type requirements are maintained because of the relatively large background for the high-yield  $K^-K^+\pi^+$  decay

TABLE IV: Measured cross sections for final states consisting of two neutral non-strange charm mesons. The first error on each cross section is statistical and the second is systematic.

$E_{\text{cm}}$ (MeV)	$\sigma(D^0\bar{D}^0)$ (pb)	$\sigma(D^{*0}\bar{D}^0)$ (pb)	$\sigma(D^{*0}\bar{D}^{*0})$ (pb)
3970	$86 \pm 29 \pm 4$	$2280 \pm 134 \pm 78$	-
3990	$133 \pm 41 \pm 6$	$2740 \pm 157 \pm 93$	-
4010	$76 \pm 25 \pm 3$	$3320 \pm 13 \pm 113$	-
4015	$< 10$ (90%C.L.)	$3840 \pm 283 \pm 131$	$213 \pm 76 \pm 9$
4030	$334 \pm 70 \pm 15$	$3200 \pm 183 \pm 109$	$2000 \pm 125 \pm 94$
4060	$410 \pm 72 \pm 18$	$2230 \pm 147 \pm 76$	$2290 \pm 132 \pm 108$
4120	$303 \pm 70 \pm 14$	$1400 \pm 135 \pm 48$	$2550 \pm 154 \pm 120$
4140	$177 \pm 40 \pm 8$	$1350 \pm 100 \pm 46$	$2443 \pm 116 \pm 115$
4160	$167 \pm 28 \pm 8$	$1252 \pm 69 \pm 43$	$2566 \pm 84 \pm 121$
4170	$177 \pm 7 \pm 8$	$1272 \pm 19 \pm 43$	$2363 \pm 19 \pm 111$
4180	$179 \pm 39 \pm 8$	$1211 \pm 92 \pm 41$	$2173 \pm 104 \pm 102$
4200	$180 \pm 55 \pm 8$	$1030 \pm 123 \pm 35$	$1830 \pm 139 \pm 86$
4260	$86 \pm 18 \pm 4$	$1080 \pm 59 \pm 37$	$269 \pm 42 \pm 13$

TABLE V: Measured cross sections for final states consisting of two charged non-strange charm mesons. The first error on each cross section is statistical and the second is systematic.

$E_{\text{cm}}$ (MeV)	$\sigma(D^+\bar{D}^-)$ (pb)	$\sigma(D^{*+}\bar{D}^-)$ (pb)	$\sigma(D^{*+}\bar{D}^{*-})$ (pb)
3970	$137 \pm 26 \pm 6$	$2230 \pm 131 \pm 76$	-
3990	$90 \pm 22 \pm 4$	$2750 \pm 156 \pm 94$	-
4010	$135 \pm 22 \pm 6$	$3300 \pm 132 \pm 112$	-
4015	$38 \pm 20 \pm 2$	$3703 \pm 274 \pm 126$	-
4030	$196 \pm 35 \pm 9$	$3300 \pm 181 \pm 112$	$1400 \pm 170 \pm 66$
4060	$480 \pm 55 \pm 22$	$2170 \pm 143 \pm 74$	$2390 \pm 222 \pm 112$
4120	$310 \pm 50 \pm 14$	$1560 \pm 136 \pm 53$	$2280 \pm 232 \pm 107$
4140	$200 \pm 29 \pm 9$	$1376 \pm 98 \pm 47$	$2556 \pm 196 \pm 120$
4160	$200 \pm 21 \pm 9$	$1376 \pm 69 \pm 47$	$2479 \pm 135 \pm 117$
4170	$182 \pm 6 \pm 8$	$1285 \pm 18 \pm 44$	$2357 \pm 19 \pm 111$
4180	$197 \pm 27 \pm 9$	$1296 \pm 87 \pm 44$	$2145 \pm 172 \pm 101$
4200	$181 \pm 36 \pm 8$	$1070 \pm 116 \pm 36$	$1564 \pm 215 \pm 74$
4260	$94 \pm 13 \pm 4$	$1022 \pm 54 \pm 35$	$237 \pm 54 \pm 11$

mode. For our energy points below 4120 MeV, where  $D_s$  production occurs only through  $D_s^+D_s^-$ , the yield is extracted by fitting  $M_{\text{bc}}$  to a Gaussian signal and ARGUS background function [19]. For 4120 MeV and above, event types involving  $D_s^{*+}$  contribute. For all candidate events that pass the selection requirements for any of  $D_s^+D_s^-$ ,  $D_s^{*+}D_s^-$ , and  $D_s^{*+}D_s^{*-}$  (the last only for 4260 MeV), a fit to the  $D_s^+$  invariant mass is used to determine the yield.

TABLE VI: Measured cross sections for final states consisting of two strange charm mesons. The first error on each cross section is statistical and the second is systematic.

$E_{\text{cm}}$ (MeV)	$\sigma(D_s^+ D_s^-)$ (pb)	$\sigma(D_s^{*+} D_s^-)$ (pb)	$\sigma(D_s^{*+} D_s^{*-})$ (pb)
3970	$102 \pm 26 \pm 6$	-	-
3990	$133 \pm 31 \pm 7$	-	-
4010	$269 \pm 30 \pm 15$	-	-
4015	$250 \pm 59 \pm 14$	-	-
4030	$174 \pm 36 \pm 10$	-	-
4060	$51 \pm 28 \pm 3$	-	-
4120	$26 \pm 26 \pm 1$	$478 \pm 64 \pm 25$	-
4140	$25 \pm 20 \pm 1$	$684 \pm 59 \pm 36$	-
4160	$< 15$ (90%C.L.)	$905 \pm 11 \pm 48$	-
4170	$34 \pm 3 \pm 2$	$916 \pm 11 \pm 49$	-
4180	$7 \pm 16 \pm 1$	$889 \pm 59 \pm 47$	-
4200	$15 \pm 22 \pm 1$	$812 \pm 82 \pm 43$	-
4260	$47 \pm 22 \pm 3$	$34 \pm 9 \pm 2$	$440 \pm 27 \pm 30$

TABLE VII: Measured cross sections for multi-body final states, consisting of two charm mesons and an extra pion, for all data points above the production threshold. The first error on each cross section is statistical and the second is systematic.

$E_{\text{cm}}$ (MeV)	$\sigma(D^* \bar{D} \pi)$ (pb)	$\sigma(D^* \bar{D}^* \pi)$ (pb)
4060	$144 \pm 94 \pm 17$	-
4120	$45 \pm 83 \pm 5$	-
4140	$412 \pm 87 \pm 49$	-
4160	$389 \pm 60 \pm 47$	-
4170	$440 \pm 20 \pm 53$	-
4180	$575 \pm 92 \pm 69$	-
4200	$735 \pm 129 \pm 88$	-
4260	$638 \pm 93 \pm 77$	$322 \pm 67 \pm 80$

The second cross-check is a determination of the total cross section made by counting multihadronic events. The contribution of  $uds$  continuum production is estimated with measurements made at  $E_{\text{cm}} = 3671$  MeV, below  $c\bar{c}$  threshold, and extrapolated as  $1/s$ . Procedures for this measurement are identical to those used to determine the cross section for  $e^+e^- \rightarrow \psi(3770) \rightarrow \text{hadrons}$  in CLEO-c data at  $E_{\text{cm}} = 3770$  MeV [20].

Fig. 6 (bottom frame) shows the inclusive measurements (statistical and systematic uncertainties combined in quadrature) and the sum of the cross sections for the measured exclusive final states without radiative corrections. The excellent agreement demonstrates that, to current precision, the measured exclusive two- and three-body final states saturate charm production in this region. Furthermore, charm is demonstrated to account for all

production of multihadronic events above the extrapolated  $uds$  cross section.

For the inclusive-charm cross-section measurements, the systematic uncertainties associated with the per-particle efficiencies for tracking and particle identification are identical to those of the exclusive measurements. The uncertainties in normalization (luminosity and branching fractions) are also identical. Systematic uncertainty in the yield extraction is dominated by the choice of fitting function. This is evaluated mode by mode and propagated into overall systematic uncertainties accounting for all correlations, with combined systematic uncertainties of  $\pm 4.3\%$ ,  $\pm 5.1\%$ , and  $\pm 8.6\%$  ( $\pm 10.6\%$ ) for  $D^0$ ,  $D^+$ , and  $D_s^+$  below (above) 4120 MeV. For the hadron-counting inclusive cross sections, the systematic uncertainties are identical to those of Ref. [20]. The systematic errors for the hadron-counting method are slightly energy-dependent, varying between 5.2% and 6.1% due to the different amounts of  $J/\psi$ ,  $\psi(2S)$ , and  $\psi(3770)$  present at each energy.

Table VIII gives the inclusive cross sections and the sum of the exclusive cross sections with both statistical and systematic uncertainties.

TABLE VIII: Comparison of the total charm cross section determined by summing the exclusive measurements (Tables IV, VI and VII) with those found by the two inclusive techniques: charm-meson counting and multihadronic-event counting. The first error on each measurement is statistical and the second systematic. The cross-section measurements are not radiatively corrected. The last column gives the value of  $R$  from the hadron-counting measurement, with radiative corrections as described in the text and correction for non-charm continuum production based on  $R_{uds} = 2.285 \pm 0.03$ , as determined by a  $\frac{1}{s}$  fit to previous  $R$  measurements between 3.2 and 3.72 GeV [23].

Energy (MeV)	Exclusive $D$ -meson (nb)	Inclusive $D$ -meson (nb)	Hadron Counting (nb)	$R$ (ISR-corrected)
3970	$4.83 \pm 0.19 \pm 0.15$	$4.91 \pm 0.18 \pm 0.16$	$4.91 \pm 0.13 \pm 0.30$	$3.36 \pm 0.04 \pm 0.05$
3990	$5.85 \pm 0.23 \pm 0.19$	$5.93 \pm 0.21 \pm 0.19$	$5.87 \pm 0.14 \pm 0.34$	$3.55 \pm 0.05 \pm 0.06$
4010	$7.10 \pm 0.14 \pm 0.23$	$7.05 \pm 0.17 \pm 0.23$	$7.21 \pm 0.12 \pm 0.40$	$3.88 \pm 0.04 \pm 0.08$
4015	$7.94 \pm 0.41 \pm 0.26$	$7.62 \pm 0.34 \pm 0.25$	$7.88 \pm 0.18 \pm 0.43$	$3.95 \pm 0.08 \pm 0.08$
4030	$10.60 \pm 0.34 \pm 0.27$	$10.87 \pm 0.28 \pm 0.37$	$11.30 \pm 0.15 \pm 0.59$	$4.74 \pm 0.07 \pm 0.12$
4060	$10.16 \pm 0.36 \pm 0.27$	$9.98 \pm 0.26 \pm 0.34$	$9.98 \pm 0.14 \pm 0.53$	$4.34 \pm 0.05 \pm 0.10$
4120	$8.95 \pm 0.37 \pm 0.25$	$9.13 \pm 0.28 \pm 0.31$	$9.43 \pm 0.15 \pm 0.49$	$4.21 \pm 0.06 \pm 0.10$
4140	$9.22 \pm 0.29 \pm 0.26$	$9.11 \pm 0.22 \pm 0.30$	$9.58 \pm 0.24 \pm 0.50$	$4.18 \pm 0.04 \pm 0.10$
4160	$9.33 \pm 0.20 \pm 0.26$	$9.10 \pm 0.15 \pm 0.30$	$9.62 \pm 0.17 \pm 0.50$	$4.18 \pm 0.03 \pm 0.10$
4170	$9.03 \pm 0.04 \pm 0.25$	$9.09 \pm 0.07 \pm 0.30$	$9.45 \pm 0.09 \pm 0.49$	$4.20 \pm 0.01 \pm 0.10$
4180	$8.67 \pm 0.27 \pm 0.24$	$8.70 \pm 0.20 \pm 0.29$	$9.07 \pm 0.12 \pm 0.47$	$4.17 \pm 0.04 \pm 0.10$
4200	$7.42 \pm 0.35 \pm 0.20$	$7.45 \pm 0.26 \pm 0.25$	$8.37 \pm 0.14 \pm 0.43$	$3.77 \pm 0.05 \pm 0.08$
4260	$4.27 \pm 0.16 \pm 0.14$	$4.20 \pm 0.10 \pm 0.14$	$4.34 \pm 0.16 \pm 0.23$	$3.06 \pm 0.02 \pm 0.04$

For comparison with other experiments and theory it is necessary to obtain Born-level cross sections from the observed cross sections by correcting for ISR. We do this by calculating correction factors following the method of Kuraev and Fadin [21], which gives the observed cross section at any  $\sqrt{s}$ :

$$\sigma_{\text{obs}}(s) = \int_0^1 dk \cdot f(k, s) \sigma_B(s_{\text{eff}}), \quad (2)$$

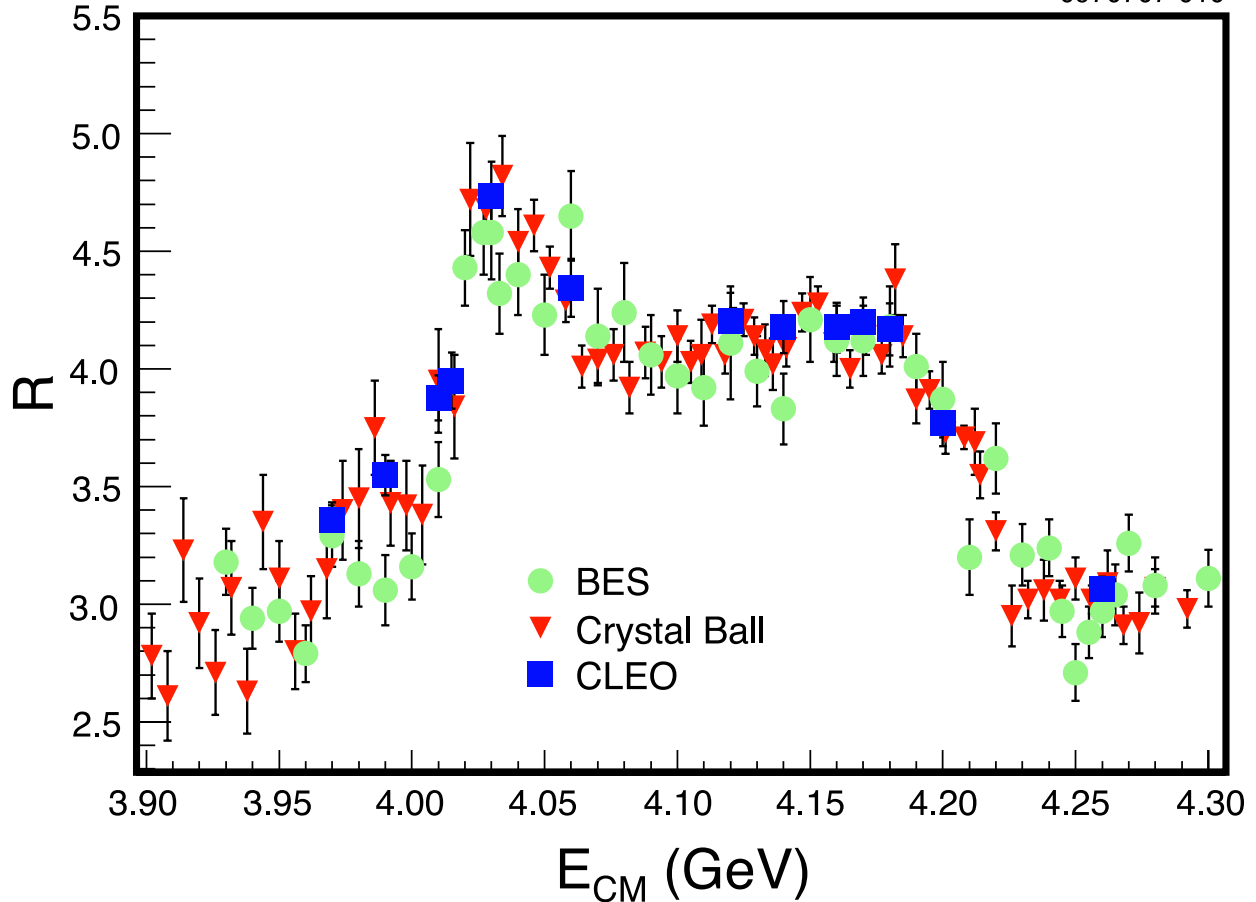


FIG. 7:  $R$  (including radiative corrections) from this analysis and from previous measurements [6, 23].

where the Born cross section  $\sigma_B$  is a function of the effective center-of-mass energy squared ( $k = (s - s_{\text{eff}})/s$ ), and  $f(k, s)$  is the ISR kernel. The radiative-correction factor is also calculated following the alternative implementation of Bonneau and Martin [22]. We take the difference between the two methods as an estimate of the underlying theoretical uncertainty in the calculation of the radiative-correction factor. We also consider systematic uncertainty due to our approximation of  $\sigma_B(s_{\text{eff}})$ , required for Eq. 2, by taking the difference between a simple linear interpolation and a fit to a sum of Breit-Wigners to both the BES [6] and Crystal Ball (CB) [23]  $R$  measurements. Fig. 7 shows that there is excellent agreement between our inclusive-charm measurement and the previous  $R$  measurements.

## VII. SUMMARY AND CONCLUSIONS

In summary, we have presented detailed information about charm production above  $c\bar{c}$  threshold. Realizing the main objective of the CLEO-c scan run, we find the center-of-mass energy that maximizes the yield of  $D_s$  to be 4170 MeV, where the cross section of  $\sim 0.9$  nb is dominantly  $D_s^{*+}D_s^-$ . This information has guided the planning of subsequent CLEO-c running, with initial results already presented on leptonic [24] and hadronic [15]  $D_s$



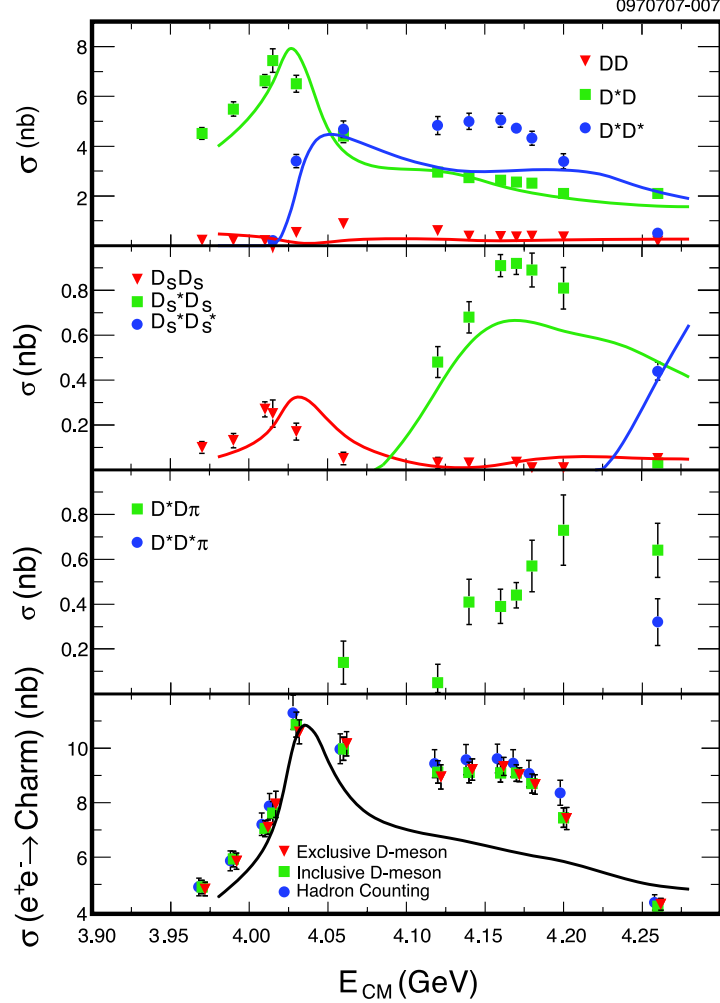


FIG. 8: Comparisons between measured cross sections and the updated predictions of the potential model of Eichten *et al.* [9, 25] (solid lines).

decays. The total charm cross section between 3.97 GeV and 4.26 GeV has been measured both inclusively and for specific two-body and multi-body final states. Internal consistency is excellent and radiatively-corrected inclusive cross sections are consistent with previous experimental results. Fig. 6 shows that the observed exclusive cross sections for  $D\bar{D}$ ,  $D^*\bar{D}$ ,  $D^*\bar{D}^*$ ,  $D_s^+D_s^-$ ,  $D_s^{*+}D_s^-$ ,  $D_s^{*+}D_s^{*-}$ ,  $D^*\bar{D}\pi$ , and  $D^*\bar{D}^*\pi$  exhibit structure that reflects the intricate behavior expected in the charm-threshold region. Fig. 8 provides a comparison between our measured cross sections and the updated calculation of Eichten *et al.* [9, 25]. There is reasonable qualitative agreement for most of the two-charm-meson final states. The most notable exception is the cross section for  $D^*\bar{D}^*$  in the region between 4050 and 4200 MeV, where the measurement exceeds the prediction by as much as 2 nb. This corresponds to nearly a factor-of-two disagreement in the ratio of  $D^*\bar{D}^*$  to  $D^*\bar{D}$  production, accounting for about two thirds of the difference in the total charm cross section. This is a much larger effect than the absence of a multi-body component from the theoretical prediction.

It has been suggested by Dubynskiy and Voloshin [26] that the existence of a peak in the  $D^*\bar{D}$  and  $D_s^+D_s^-$  channels at the  $D^*\bar{D}^*$  threshold, along with the observation that there is a minimum in  $D\bar{D}$ , in agreement with recent results from BaBar [27], can be interpreted as a

possible new narrow resonance, but available data are insufficient for a definitive assessment.

The  $D^*\bar{D}^*$  cross section exhibits a plateau just above its threshold. This contrasts with  $D^*\bar{D}$ , which we observe to peak at threshold, in agreement with recent results from Belle [28].

Studies of open-charm production at 4260 MeV have the potential to discriminate among possible explanations of the nature of the  $Y(4260)$ . For example, hybrid charmonium models predict a large coupling to the wide  $D_1(2430)^0\bar{D}^0$  and a small one to  $D_s^+D_s^-$  [29]. A tetraquark interpretation suggests a large decay to  $D\bar{D}$  or  $D_s^+D_s^-$  [29, 30, 31]. Complicated threshold effects could lead to enhancement of the  $D^*\pi$  final state through off-shell production of  $D_1$  [32]. Tables IV, VI and VII show no evidence for enhancement of the cross section for any open-charm final states at 4260 MeV. CLEO-c has previously confirmed the  $Y(4260)$  through its decay to  $\pi^+\pi^-J/\psi$ , measuring  $\sigma(\pi^+\pi^-J/\psi) = 58_{-10}^{+12} \pm 4$  pb [2]. Under the assumption that all open-charm production is accounted for by  $Y(4260)$  decays, it is possible to set conservative upper limits on the ratio of the cross section for production of  $Y(4260)$  and decay to our measured open-charm states to that for production and decay to  $\pi^+\pi^-J/\psi$ . Table IX provides a compilation of these limits. The lack of obvious enhance-

TABLE IX: Upper limits (90% confidence level) on the ratio of the cross section for production of  $Y(4260)$  and decay to our measured open-charm states at 4260 MeV to that for production of  $Y(4260)$  and decay to  $\pi^+\pi^-J/\psi$ .

Final State ( $X$ )	$\frac{\sigma(Y(4260) \rightarrow X)}{\sigma(Y(4260) \rightarrow \pi^+\pi^-J/\psi)}$
$D\bar{D}$	$< 4.0$
$D^*\bar{D}$	$< 45$
$D^*\bar{D}^*$	$< 11$
$D^*\bar{D}\pi$	$< 15$
$D^*\bar{D}^*\pi$	$< 8.2$
$D_s^+D_s^-$	$< 1.3$
$D_s^{*+}D_s^-$	$< 0.8$
$D_s^{*+}D_s^{*-}$	$< 9.5$

ment in any open-charm channel relative to other energies, which is in stark contrast to the clear enhancement in  $\pi^+\pi^-J/\psi$ , tends to disfavor the hybrid charmonium and tetraquark proposals. More definitive statements will require additional data from future experiments.

## VIII. ACKNOWLEDGMENTS

We gratefully acknowledge the effort of the CESR staff in providing us with excellent luminosity and running conditions. We thank E. Eichten and M. Voloshin for useful discussions. D. Cronin-Hennessy and A. Ryd thank the A.P. Sloan Foundation. This work was supported by the National Science Foundation, the U.S. Department of Energy, the Natural Sciences and Engineering Research Council of Canada, and the U.K. Science and

- 
- [1] B. Aubert *et al.* (BaBar Collaboration), Phys. Rev. Lett. **95**, 142001 (2005).
  - [2] T. E. Coan *et al.* (CLEO Collaboration), Phys. Rev. Lett. **96**, 162003 (2006).
  - [3] C. Z. Yuan *et al.* (Belle Collaboration), Phys. Rev. Lett. **99**, 182004 (2007).
  - [4] M. Kobayashi and T. Maskawa, Prog. Theor. Phys. **49**, 652 (1973).
  - [5] S. Eidelman *et al.* (Particle Data Group), Phys. Lett. B **592**, 1 (2004).
  - [6] J. Z. Bai *et al.* (BES Collaboration), Phys. Rev. Lett. **88**, 101802 (2002).
  - [7] T. Barnes, J. Phys. Conf. Ser. **9**, 127 (2005).
  - [8] T. Barnes, arXiv:hep-ph/0406327.
  - [9] E. Eichten, K. Gottfried, T. Kinoshita, K.D. Lane, and T.M. Yan, Phys. Rev. D **21**, 203 (1980).
  - [10] M. B. Voloshin, arXiv:hep-ph/0602233.
  - [11] R. A. Briere *et al.* (CESR-c and CLEO-c Taskforces, CLEO-c Collaboration), Cornell University, LEPP Report No. CLNS 01/1742 (2001) (unpublished).
  - [12] Q. He *et al.* (CLEO Collaboration), Phys. Rev. Lett. **95**, 121801 (2005) (Erratum-*ibid.* **96**, 199903 (2006)).
  - [13] S. Dobbs *et al.* (CLEO Collaboration), Phys. Rev. D **76**, 112001 (2007).
  - [14] Y. Kubota *et al.* (CLEO Collaboration), Nucl. Instrum. Meth. A **320**, 66 (1992); M. Artuso *et al.*, *ibid.* **554**, 147 (2005); D. Peterson *et al.*, *ibid.* **478**, 142 (2002).
  - [15] J. Alexander *et al.* [CLEO Collaboration], submitted to Phys. Rev. Lett., arXiv:0801.0680 [hep-ex].
  - [16] R. Brun *et al.*, GEANT 3.21, CERN Program Library Long Writeup W5013, unpublished.
  - [17] D. J. Lange, Nucl. Instrum. Meth. A **462**, 152 (2001).
  - [18] B. W. Lang, Ph.D. thesis, University of Minnesota, arXiv:0801.1092v1 [hep-ex].
  - [19] H. Albrecht *et al.* (ARGUS Collaboration), Phys. Lett. B **241**, 278 (1990).
  - [20] D. Besson *et al.* (CLEO Collaboration), Phys. Rev. Lett. **96**, 092002 (2006).
  - [21] E. A. Kuraev and V. S. Fadin, Sov. J. Nucl. Phys. **41**, 466 (1985) (Yad. Fiz. **41**, 733 (1985)).
  - [22] G. Bonneau and F. Martin, Nucl. Phys. B **27**, 381 (1971).
  - [23] A. Osterheld *et al.*, SLAC-PUB-4160 (1986).
  - [24] M. Artuso *et al.* (CLEO Collaboration), Phys. Rev. Lett. **99**, 071802 (2007).
  - [25] E. Eichten, “New States above Charm Threshold,” talk presented at the International Workshop on Heavy Quarkonium, Brookhaven National Laboratory, June, 2006, and private communication.
  - [26] S. Dubynskiy and M. B. Voloshin, Mod. Phys. Lett. A **21**, 2779 (2006).
  - [27] B. Aubert *et al.* (BaBar Collaboration), Phys. Rev. D **76**, 111105 (2007).
  - [28] K. Abe *et al.* (Belle Collaboration), arXiv:0708.0082 [hep-ex]; K. Abe *et al.* (Belle Collaboration), Phys. Rev. Lett. **98**, 092001 (2007).
  - [29] F. E. Close and P. R. Page, Phys. Lett. B **628**, 215 (2005).
  - [30] D. Ebert, R. N. Faustov and V. O. Galkin, Phys. Lett. B **634**, 214 (2006).
  - [31] L. Maiani, V. Riquer, F. Piccinini and A. D. Polosa, Phys. Rev. D **72**, 031502(R) (2005).
  - [32] J. L. Rosner, Phys. Rev. D **74**, 076006 (2006).